EUROPEAN ORGANIZATION FOR NUCLEAR RESEARCH

CERN–EP/98–189

30 November 1998

Measurement of $A_{FB}^{b\bar{b}}$ in Hadronic Z Decays using a Jet Charge Technique

DELPHI Collaboration

Abstract

The $b\bar{b}$ forward-backward asymmetry has been determined from the average charge flow measured in a sample of 3,500,000 hadronic Z decays collected with the DELPHI detector in 1992 - 1995. The measurement is performed in an enriched $b\bar{b}$ sample selected using an impact parameter tag and results in the following values for the $b\bar{b}$ forward-backward asymmetry:

$$\begin{aligned} A_{FB}^{b\bar{b}}\ (89.55\ \text{GeV}) &= 0.068 \pm 0.018\ (\text{stat.}) \pm 0.0013(\text{syst.}) \\ A_{FB}^{b\bar{b}}\ (91.26\ \text{GeV}) &= 0.0982 \pm 0.0047(\text{stat.}) \pm 0.0016(\text{syst.}) \\ A_{FB}^{b\bar{b}}\ (92.94\ \text{GeV}) &= 0.123 \pm 0.016\ (\text{stat.}) \pm 0.0027(\text{syst.}) \end{aligned}$$

The $b\bar{b}$ charge separation required for this analysis is directly measured in the b tagged sample, while the other charge separations are obtained from a fragmentation model precisely calibrated to data. The effective weak mixing angle is deduced from the measurement to be:

$$\sin^2\theta^{l}_{\text{eff}} = 0.23186 \pm 0.00083$$

(Submitted to Eur. Phys. J. C)

P.Abreu[21], W.Adam[50], T.Adye[36], P.Adzic[11], Z.Albrecht[17], T.Aldeweireld[2], G.D.Alekseev[16], R.Alemany[49], T.Allmendinger[17], P.P.Allport[22], S.Almehed[24], U.Amaldi[9], S.Amato[47], E.G.Anassontzis[3], P.Andersson[44], A.Andreazza[9], S.Andringa[21], P.Antilogus[25], W-D.Apel[17], Y.Arnoud[14], B.Åsman[44], J-E.Augustin[25], A.Augustinus[9], P.Baillon[9], P.Bambade[19], F.Barao[21], G.Barbiellini[46], R.Barbier[25], D.Y.Bardin[16], G.Barker[9], A.Baroncelli[38], M.Battaglia[15], M.Baubillier[23], K-H.Becks[52], M.Begalli[6], P.Beilliere[8], Yu.Belokopytov[9,53], K.Belous[42], A.C.Benvenuti[5], C.Berat[14], M.Berggren[25], D.Bertini[25], D.Bertrand[2], M.Besancon[39], F.Bianchi[45], M.Bigi[45], M.S.Bilenky[16], M-A.Bizouard[19], D.Bloch[10], H.M.Blom[30], M.Bonesini[27], W.Bonivento[27], M.Boonekamp[39], P.S.L.Booth[22], A.W.Borgland[4], G.Borisov[19], C.Bosio[41], O.Botner[48], E.Boudinov[30], B.Bouquet[19], C.Bourdarios[19], T.J.V.Bowcock[22], I.Boyko[16], I.Bozovic[11], M.Bozzo[13], P.Branchini[38], T.Brenke[52], R.A.Brenner[48], P.Bruckman[18], J-M.Brunet[8], L.Bugge[32], T.Buran[32], T.Burgsmueller[52], P.Buschmann[52], S.Cabrera[49], M.Caccia[27], M.Calvi[27], A.J.Camacho Rozas[40], T.Camporesi[9], V.Canale[37], F.Carena[9], L.Carroll[22], C.Caso[13], M.V.Castillo Gimenez[49], A.Cattai[9], F.R.Cavallo[5], V.Chabaud[9], M.Chapkin[42], Ph.Charpentier[9], L.Chaussard[25], P.Checchia[35], G.A.Chelkov[16], R.Chierici[45], P.Chliapnikov[42], P.Chochula[7], V.Chorowicz[25], J.Chudoba[29], P.Collins[9], R.Contri[13], E.Cortina[49], G.Cosme[19], F.Cossutti[39], J-H.Cowell[22], H.B.Crawley[1], D.Crennell[36], G.Crosetti[13], J.Cuevas Maestro[33], S.Czellar[15], G.Damgaard[28], M.Davenport[9], W.Da Silva[23], A.Deghorain[2], G.Della Ricca[46], P.Delpierre[26], N.Demaria[9], A.De Angelis[9], W.De Boer[17], S.De Brabandere[2], C.De Clercq[2], B.De Lotto[46], A.De Min[35], L.De Paula[47], H.Dijkstra[9], L.Di Ciaccio[37], J.Dolbeau[8], K.Doroba[51], M.Dracos[10], J.Drees[52], M.Dris[31], A.Duperrin[25], J-D.Durand[25,9], G.Eigen[4], T.Ekelof[48], G.Ekspong[44], M.Ellert[48], M.Elsing[9], J-P.Engel[10], B.Erzen[43], M.Espirito Santo[21], E.Falk[24], G.Fanourakis[11], D.Fassouliotis[11], J.Fayot[23], M.Feindt[17], A.Fenyuk[42], P.Ferrari[27], A.Ferrer[49], E.Ferrer-Ribas[19], S.Fichet[23], A.Firestone[1], P.-A.Fischer[9], U.Flagmeyer[52], H.Foeth[9], E.Fokitis[31], F.Fontanelli[13], B.Franek[36], A.G.Frodesen[4], R.Fruhwirth[50], F.Fulda-Quenzer[19], J.Fuster[49], A.Galloni[22], D.Gamba[45], S.Gamblin[19], M.Gandelman[47], C.Garcia[49], J.Garcia[40], C.Gaspar[9], M.Gaspar[47], U.Gasparini[35], Ph.Gavillet[9], E.N.Gazis[31], D.Gele[10], N.Ghodbane[25], I.Gil[49], F.Glege[52], R.Gokieli[51], B.Golob[43], G.Gomez-Ceballos[40], P.Goncalves[21], I.Gonzalez Caballero[40], G.Gopal[36], L.Gorn[1,54], M.Gorski[51], Yu.Gouz[42], V.Gracco[13], J.Grahl[1], E.Graziani[38], C.Green[22], H-J.Grimm[17], P.Gris[39], G.Grosdidier[19], K.Grzelak[51], M.Gunther[48], J.Guy[36], F.Hahn[9], S.Hahn[52], S.Haider[9], A.Hallgren[48], K.Hamacher[52], F.J.Harris[34], V.Hedberg[24], S.Heising[17], J.J.Hernandez[49], P.Herquet[2], H.Herr[9], T.L.Hessing[34], J.-M.Heuser[52], E.Higon[49], S-O.Holmgren[44], P.J.Holt[34], D.Holthuizen[30], S.Hoorelbeke[2], M.Houlden[22], J.Hrubec[50], K.Huet[2], G.J.Hughes[22], K.Hultqvist[44], J.N.Jackson[22], R.Jacobsson[9], P.Jalocha[9], R.Janik[7], Ch.Jarlskog[24], G.Jarlskog[24], P.Jarry[39], B.Jean-Marie[19], E.K.Johansson[44], P.Jonsson[25], C.Joram[9], P.Juillot[10], F.Kapusta[23], K.Karafasoulis[11], S.Katsanevas[25], E.C.Katsoufis[31], R.Keranen[17], B.P.Kersevan[43], B.A.Khomenko[16], N.N.Khovanski[16], A.Kiiskinen[15], B.King[22], A.Kinvig[22], N.J.Kjaer[30], O.Klapp[52], H.Klein[9], P.Kluit[30], P.Kokkinias[11], M.Koratzinos[9], V.Kostioukhine[42], C.Kourkoumelis[3], O.Kouznetsov[16], M.Krammer[50], C.Kreuter[9], E.Kriznic[43], J.Krstic[11], Z.Krumstein[16], P.Kubinec[7], W.Kucewicz[18], J.Kurowska[51], K.Kurvinen[15], J.W.Lamsa[1], D.W.Lane[1], P.Langefeld[52], V.Lapin[42], J-P.Laugier[39], R.Lauhakangas[15], G.Leder[50], F.Ledroit[14], V.Lefebure[2], L.Leinonen[44], A.Leisos[11], R.Leitner[29], G.Lenzen[52], V.Lepeltier[19], T.Lesiak[18], M.Lethuillier[39], J.Libby[34], D.Liko[9], A.Lipniacka[44], I.Lippi[35], B.Loerstad[24], J.G.Loken[34], J.H.Lopes[47], J.M.Lopez[40], R.Lopez-Fernandez[14], D.Loukas[11], P.Lutz[39], L.Lyons[34], J.MacNaughton[50], J.R.Mahon[6], A.Maio[21], A.Malek[52], T.G.M.Malmgren[44], V.Malychev[16], F.Mandl[50], J.Marco[40], R.Marco[40], B.Marechal[47], M.Margoni[35], J-C.Marin[9], C.Mariotti[9], A.Markou[11], C.Martinez-Rivero[19], F.Martinez-Vidal[49], S.Marti i Garcia[9], N.Mastroyiannopoulos[11], F.Matorras[40], C.Matteuzzi[27], G.Matthiae[37], J.Mazik[29], F.Mazzucato[35], M.Mazzucato[35], M.Mc Cubbin[22], R.Mc Kay[1], R.Mc Nulty[22], G.Mc Pherson[22], C.Meroni[27], W.T.Meyer[1], E.Migliore[45], L.Mirabito[25], U.Mjoernmark[24], T.Moa[44], M.Moch[17], R.Moeller[28], K.Moenig[9], M.R.Monge[13], X.Moreau[23], P.Morettini[13], G.Morton[34], U.Mueller[52], K.Muenich[52], M.Mulders[30], C.Mulet-Marquis[14], R.Muresan[24], W.J.Murray[36], B.Muryn[14,18], G.Myatt[34], T.Myklebust[32], F.Naraghi[14], F.L.Navarria[5], S.Navas[49], K.Nawrocki[51], P.Negri[27], S.Nemecek[12], N.Neufeld[9], N.Neumeister[50], R.Nicolaidou[14], B.S.Nielsen[28], M.Nikolenko[10,16], V.Nomokonov[15], A.Normand[22], A.Nygren[24], V.Obraztsov[42], A.G.Olshevski[16], A.Onofre[21], R.Orava[15], G.Orazi[10], K.Osterberg[15], A.Ouraou[39], M.Paganoni[27], S.Paiano[5], R.Pain[23], R.Paiva[21], J.Palacios[34], H.Palka[18], Th.D.Papadopoulou[31], K.Papageorgiou[11], L.Pape[9], C.Parkes[34], F.Parodi[13], U.Parzefall[22], A.Passeri[38], O.Passon[52], M.Pegoraro[35], L.Peralta[21], M.Pernicka[50], A.Perrotta[5], C.Petridou[46], A.Petrolini[13], H.T.Phillips[36], F.Pierre[39], M.Pimenta[21], E.Piotto[27], T.Podobnik[43], M.E.Pol[6], G.Polok[18], P.Poropat[46], V.Pozdniakov[16], P.Privitera[37], N.Pukhaeva[16], A.Pullia[27], D.Radojicic[34], S.Ragazzi[27], H.Rahmani[31], D.Rakoczy[50], P.N.Ratoff[20], A.L.Read[32], P.Rebecchi[9], N.G.Redaelli[27], M.Regler[50], D.Reid[9], R.Reinhardt[52], P.B.Renton[34], L.K.Resvanis[3], F.Richard[19], J.Ridky[12], G.Rinaudo[45], O.Rohne[32], A.Romero[45], P.Ronchese[35], E.I.Rosenberg[1], P.Rosinsky[7], P.Roudeau[19], T.Rovelli[5], Ch.Royon[39], V.Ruhlmann-Kleider[39], A.Ruiz[40], H.Saarikko[15], Y.Sacquin[39], A.Sadovsky[16], G.Sajot[14], J.Salt[49], D.Sampsonidis[11], M.Sannino[13], H.Schneider[17], Ph.Schwemling[23], U.Schwickerath[17], M.A.E.Schyns[52], F.Scuri[46], P.Seager[20], Y.Sedykh[16], A.M.Segar[34], R.Sekulin[36], R.C.Shellard[6], A.Sheridan[22], M.Siebel[52], L.Simard[39], F.Simonetto[35], A.N.Sisakian[16], T.B.Skaali[32], G.Smadja[25], N.Smirnov[42], O.Smirnova[24], G.R.Smith[36], A.Sopczak[17], R.Sosnowski[51], T.Spassov[21], E.Spiriti[38], P.Sponholz[52], S.Squarcia[13], D.Stampfer[50], C.Stanescu[38], S.Stanic[43], S.Stapnes[32], K.Stevenson[34], A.Stocchi[19], J.Strauss[50], R.Strub[10], B.Stugu[4], M.Szczekowski[51], M.Szeptycka[51], T.Tabarelli[27], F.Tegenfeldt[48], F.Terranova[27], J.Thomas[34], A.Tilquin[26], J.Timmermans[30], N.Tinti[5], L.G.Tkatchev[16],

S.Todorova[10], D.Z.Toet[30], B.Tome[21], A.Tonazzo[27], L.Tortora[38], G.Transtromer[24], D.Treille[9], G.Tristram[8], M.Trochimczuk[51], C.Troncon[27], A.Tsirou[9], M-L.Turluer[39], I.A.Tyapkin[16], S.Tzamarias[11], B.Ueberschaer[52], O.Ullaland[9], V.Uvarov[42], G.Valenti[5], E.Vallazza[46], G.W.Van Apeldoorn[30], P.Van Dam[30], J.Van Eldik[30], A.Van Lysebetten[2], I.Van Vulpen[30], N.Vassilopoulos[34], G.Vegni[27], L.Ventura[35], W.Venus[36], F.Verbeure[2], M.Verlato[35], L.S.Vertogradov[16], V.Verzi[37], D.Vilanova[39], L.Vitale[46], E.Vlasov[42], A.S.Vodopyanov[16], C.Vollmer[17], G.Voulgaris[3], V.Vrba[12], H.Wahlen[52], C.Walck[44], C.Weiser[17], D.Wicke[52], J.H.Wickens[2], G.R.Wilkinson[9], M.Winter[10], M.Witek[18], G.Wolf[9], J.Yi[1], O.Yushchenko[42], A.Zaitsev[42], A.Zalewska[18], P.Zalewski[51], D.Zavrtanik[43], E.Zevgolatakos[11], N.I.Zimin[16,24], G.C.Zucchelli[44], G.Zumerle[35]

[1] Department of Physics and Astronomy, Iowa State University, Ames IA 50011-3160, USA
[2] Physics Department, Univ. Instelling Antwerpen, Universiteitsplein 1, BE-2610 Wilrijk, Belgium
and IIHE, ULB-VUB, Pleinlaan 2, BE-1050 Brussels, Belgium
and Faculté des Sciences, Univ. de l'Etat Mons, Av. Maistriau 19, BE-7000 Mons, Belgium
[3] Physics Laboratory, University of Athens, Solonos Str. 104, GR-10680 Athens, Greece
[4] Department of Physics, University of Bergen, Allégaten 55, NO-5007 Bergen, Norway
[5] Dipartimento di Fisica, Università di Bologna and INFN, Via Irnerio 46, IT-40126 Bologna, Italy
[6] Centro Brasileiro de Pesquisas Físicas, rua Xavier Sigaud 150, BR-22290 Rio de Janeiro, Brazil
and Depto. de Física, Pont. Univ. Católica, C.P. 38071 BR-22453 Rio de Janeiro, Brazil
and Inst. de Física, Univ. Estadual do Rio de Janeiro, rua São Francisco Xavier 524, Rio de Janeiro, Brazil
[7] Comenius University, Faculty of Mathematics and Physics, Mlynska Dolina, SK-84215 Bratislava, Slovakia
[8] Collège de France, Lab. de Physique Corpusculaire, IN2P3-CNRS, FR-75231 Paris Cedex 05, France
[9] CERN, CH-1211 Geneva 23, Switzerland
[10] Institut de Recherches Subatomiques, IN2P3 - CNRS/ULP - BP20, FR-67037 Strasbourg Cedex, France
[11] Institute of Nuclear Physics, N.C.S.R. Demokritos, P.O. Box 60228, GR-15310 Athens, Greece
[12] FZU, Inst. of Phys. of the C.A.S. High Energy Physics Division, Na Slovance 2, CZ-180 40, Praha 8, Czech Republic
[13] Dipartimento di Fisica, Università di Genova and INFN, Via Dodecaneso 33, IT-16146 Genova, Italy
[14] Institut des Sciences Nucléaires, IN2P3-CNRS, Université de Grenoble 1, FR-38026 Grenoble Cedex, France
[15] Helsinki Institute of Physics, HIP, P.O. Box 9, FI-00014 Helsinki, Finland
[16] Joint Institute for Nuclear Research, Dubna, Head Post Office, P.O. Box 79, RU-101 000 Moscow, Russian Federation
[17] Institut für Experimentelle Kernphysik, Universität Karlsruhe, Postfach 6980, DE-76128 Karlsruhe, Germany
[18] Institute of Nuclear Physics and University of Mining and Metalurgy, Ul. Kawiory 26a, PL-30055 Krakow, Poland
[19] Université de Paris-Sud, Lab. de l'Accélérateur Linéaire, IN2P3-CNRS, Bât. 200, FR-91405 Orsay Cedex, France
[20] School of Physics and Chemistry, University of Lancaster, Lancaster LA1 4YB, UK
[21] LIP, IST, FCUL - Av. Elias Garcia, 14-1^{o}, PT-1000 Lisboa Codex, Portugal
[22] Department of Physics, University of Liverpool, P.O. Box 147, Liverpool L69 3BX, UK
[23] LPNHE, IN2P3-CNRS, Univ. Paris VI et VII, Tour 33 (RdC), 4 place Jussieu, FR-75252 Paris Cedex 05, France
[24] Department of Physics, University of Lund, Sölvegatan 14, SE-223 63 Lund, Sweden
[25] Université Claude Bernard de Lyon, IPNL, IN2P3-CNRS, FR-69622 Villeurbanne Cedex, France
[26] Univ. d'Aix - Marseille II - CPP, IN2P3-CNRS, FR-13288 Marseille Cedex 09, France
[27] Dipartimento di Fisica, Università di Milano and INFN, Via Celoria 16, IT-20133 Milan, Italy
[28] Niels Bohr Institute, Blegdamsvej 17, DK-2100 Copenhagen Ø, Denmark
[29] NC, Nuclear Centre of MFF, Charles University, Areal MFF, V Holesovickach 2, CZ-180 00, Praha 8, Czech Republic
[30] NIKHEF, Postbus 41882, NL-1009 DB Amsterdam, The Netherlands
[31] National Technical University, Physics Department, Zografou Campus, GR-15773 Athens, Greece
[32] Physics Department, University of Oslo, Blindern, NO-1000 Oslo 3, Norway
[33] Dpto. Fisica, Univ. Oviedo, Avda. Calvo Sotelo s/n, ES-33007 Oviedo, Spain
[34] Department of Physics, University of Oxford, Keble Road, Oxford OX1 3RH, UK
[35] Dipartimento di Fisica, Università di Padova and INFN, Via Marzolo 8, IT-35131 Padua, Italy
[36] Rutherford Appleton Laboratory, Chilton, Didcot OX11 OQX, UK
[37] Dipartimento di Fisica, Università di Roma II and INFN, Tor Vergata, IT-00173 Rome, Italy
[38] Dipartimento di Fisica, Università di Roma III and INFN, Via della Vasca Navale 84, IT-00146 Rome, Italy
[39] DAPNIA/Service de Physique des Particules, CEA-Saclay, FR-91191 Gif-sur-Yvette Cedex, France
[40] Instituto de Fisica de Cantabria (CSIC-UC), Avda. los Castros s/n, ES-39006 Santander, Spain
[41] Dipartimento di Fisica, Università degli Studi di Roma La Sapienza, Piazzale Aldo Moro 2, IT-00185 Rome, Italy
[42] Inst. for High Energy Physics, Serpukov P.O. Box 35, Protvino, (Moscow Region), Russian Federation
[43] J. Stefan Institute, Jamova 39, SI-1000 Ljubljana, Slovenia and Laboratory for Astroparticle Physics,
Nova Gorica Polytechnic, Kostanjeviska 16a, SI-5000 Nova Gorica, Slovenia,
and Department of Physics, University of Ljubljana, SI-1000 Ljubljana, Slovenia
[44] Fysikum, Stockholm University, Box 6730, SE-113 85 Stockholm, Sweden
[45] Dipartimento di Fisica Sperimentale, Università di Torino and INFN, Via P. Giuria 1, IT-10125 Turin, Italy
[46] Dipartimento di Fisica, Università di Trieste and INFN, Via A. Valerio 2, IT-34127 Trieste, Italy
and Istituto di Fisica, Università di Udine, IT-33100 Udine, Italy
[47] Univ. Federal do Rio de Janeiro, C.P. 68528 Cidade Univ., Ilha do Fundão BR-21945-970 Rio de Janeiro, Brazil
[48] Department of Radiation Sciences, University of Uppsala, P.O. Box 535, SE-751 21 Uppsala, Sweden
[49] IFIC, Valencia-CSIC, and D.F.A,M.N., U. de Valencia, Avda. Dr. Moliner 50, ES-46100 Burjassot (Valencia), Spain
[50] Institut für Hochenergiephysik, Österr. Akad. d. Wissensch., Nikolsdorfergasse 18, AT-1050 Vienna, Austria
[51] Inst. Nuclear Studies and University of Warsaw, Ul. Hoza 69, PL-00681 Warsaw, Poland
[52] Fachbereich Physik, University of Wuppertal, Postfach 100 127, DE-42097 Wuppertal, Germany
[53] On leave of absence from IHEP Serpukhov
[54] Now at University of Florida

1 Introduction

The coupling of the Z boson to fermions results in an asymmetric polar angular distribution of the $\mathrm{f\bar{f}}$ final states. In terms of the vector and axial vector couplings $(v_\mathrm{f}, a_\mathrm{f})$, the Standard Model predicts for pure Z exchange to the lowest order:

$$A_{FB}^{0,\mathrm{f\bar{f}}} = \frac{3}{4} \frac{2a_\mathrm{e}v_\mathrm{e}}{a_\mathrm{e}^2 + v_\mathrm{e}^2} \frac{2a_\mathrm{f}v_\mathrm{f}}{a_\mathrm{f}^2 + v_\mathrm{f}^2} \tag{1}$$

where $A_{FB}^{0,\mathrm{f\bar{f}}}$ is the forward-backward asymmetry of the $\mathrm{f\bar{f}}$ final state.

Higher order electroweak corrections can be accounted for by means of an improved Born approximation, which leaves the above relation unchanged but defines the modified couplings $\bar{a}_\mathrm{f}$, $\bar{v}_\mathrm{f}$, and an effective mixing angle $\theta_\mathrm{eff}^\mathrm{f}$ for which

$$\frac{\bar{v}_\mathrm{f}}{\bar{a}_\mathrm{f}} = 1 - 4|q_\mathrm{f}| \sin^2 \theta_\mathrm{eff}^\mathrm{f} \tag{2}$$

where q_f is the fermion electric charge. Therefore $\sin^2\theta_\mathrm{eff}^\mathrm{f}$ includes higher order effects, and its measurement is an important test of the Standard Model predictions.

It is advantageous to measure asymmetries for quark final states as the sensitivity to the initial state couplings is in principle larger than in lepton final states. Therefore these measurements determine $\sin^2\theta_\mathrm{eff}^\mathrm{l}$ as defined by the electron couplings [1], assuming lepton universality. In addition the sensitivity to $\sin^2\theta_\mathrm{eff}^\mathrm{l}$ for down type quarks is larger than for up type quarks.

Information on the original quark charges for these events has to be obtained from the final state hadrons. In this paper a momentum weighted average of the particle charges detected in one hemisphere was used. The difference Q_{FB} (often called *charge flow*) between the forward and backward hemisphere charges in each event, turns out to be a linear combination of the quark asymmetries, with coefficients mainly given by the charge separations δ_f, i.e. the quark-antiquark separation power of the hemisphere charge for each individual flavour. Any measurement of $\langle Q_{FB} \rangle$ and of the δ_f's then implies a measurement of $\sin^2\theta_\mathrm{eff}^\mathrm{l}$. Flavour tagging techniques can give access to single flavour asymmetries.

In this paper the measurement of $\langle Q_{FB} \rangle$ using a $\mathrm{b\bar{b}}$ enriched sample is presented. The $\mathrm{b\bar{b}}$ forward-backward asymmetry, $A_{FB}^{\mathrm{b\bar{b}}}$, has been determined from this measurement and the effective weak mixing angle, $\sin^2\theta_\mathrm{eff}^\mathrm{l}$, was derived.

In this section a short discussion of the principles underlying the jet charge technique and the basic definitions which will be used throughout the paper are given. The DELPHI detector and the event selection are described in section 2, together with the b-tagging technique used to obtain $\mathrm{b\bar{b}}$ enriched samples. In section 3 the determinations of the individual charge separations are described: δ_b was directly measured from the data, while the other charge separations $\delta_\mathrm{d,u,s,c}$ were obtained from an analytic model accounting for possible fragmentation model parameter variations. In section 4 the $A_{FB}^{\mathrm{b\bar{b}}}$ extraction is described, and the systematic errors are discussed in section 5. Finally a summary and conclusion are presented in section 6.

In order to measure charge asymmetries in the process $\mathrm{e^+e^-} \to \mathrm{Z} \to \mathrm{q\bar{q}} \to$ jets it is necessary to determine the charge of the quarks underlying hadron jets in an event. The quark charge has to be determined from the final state hadrons and therefore this information is diluted by the fragmentation process. Experimentally the charge of the initial fermion in the related hemisphere is estimated using the following hemisphere charge definition:

$$Q_{F(B)} = \frac{\sum_i q_i |\vec{p_i} \cdot \vec{T}|^\kappa}{\sum_i |\vec{p_i} \cdot \vec{T}|^\kappa} \qquad \begin{array}{ll} F : \vec{p_i} \cdot \vec{T} > 0 & \text{forward hemisphere} \\ B : \vec{p_i} \cdot \vec{T} < 0 & \text{backward hemisphere} \end{array} \tag{3}$$

where the sum runs over the charged tracks. $\vec{T}$ is the Thrust unit vector, q_i the particle charge, $\vec{p_i}$ the particle momentum and the exponent κ a positive number. The Thrust axis is computed using charged and neutral particles. The plane perpendicular to this axis divides each event into two hemispheres. The Thrust axis orientation was always chosen to be that nearer to the direction of the incoming electrons.

The observable, $Q_{F(B)}$, is robust against mismeasurement of the hadron momenta $\vec{p_i}$. Its value is bound in the interval -1 to 1. The projection of the hadron momenta to the Thrust axis $\vec{T}$ mainly eliminates the influence of hard gluon radiation.

For every event two quantities the charge flow, Q_{FB}, and total charge, Q_{TOT}, can be defined:

$$Q_{FB} = Q_F - Q_B \tag{4}$$

$$Q_{TOT} = Q_F + Q_B \tag{5}$$

Except for detector influences (mainly hadronic re-interaction) the average total charge $\langle Q_{TOT} \rangle$ is expected to vanish, while the average charge flow $\langle Q_{FB} \rangle$ relates to the relevant quark asymmetries:

$$\langle Q_{FB} \rangle = \sum_{flavours\ \mathrm{f}} \eta_\mathrm{f} \delta_\mathrm{f} P_\mathrm{f} A_{FB}^{\mathrm{f\bar{f}}}. \tag{6}$$

P_f is the relative abundance of a quark flavour f in the hadronic event sample. η_f is a weighting factor to account mainly for the incomplete angular acceptance, limited angular resolution and other detector effects, but also for effects of gluon radiation.

The overall impact of fragmentation of an event of quark flavour f can be estimated from the average difference of the hemisphere charge in the hemisphere of the quark f and the anti-quark $\bar{\mathrm{f}}$:

$$\delta_\mathrm{f}(\kappa) = \langle Q_\mathrm{f} - Q_{\bar{\mathrm{f}}} \rangle (\kappa) \tag{7}$$

This quantity is called charge separation, δ_f. If quarks could be directly observed $\delta_\mathrm{f} = 2q_\mathrm{f}$. In case of a pure flavour sample, which is approximately the case for the b tagged sample, δ_f can be measured from the data using the relation:

$$\delta_\mathrm{f}^2 = (\sigma_{FB}^\mathrm{f})^2 - (\sigma_{TOT}^\mathrm{f})^2 \tag{8}$$

Here $(\sigma_{FB}^\mathrm{f})^2$ and $(\sigma_{TOT}^\mathrm{f})^2$ are the variances of the Q_{FB} distribution, respectively Q_{TOT}. The validity of this equation can be seen from Fig.1. Note, however, that charge correlations between the event hemispheres and the small term $\langle Q_{FB}^\mathrm{f} \rangle^2$ are neglected in this expression.

To measure $A_{FB}^{\mathrm{b\bar{b}}}$, Eqn.6 was used, and all quantities appearing in it were evaluated. $\langle Q_{FB} \rangle$ was directly measured from the data. The b-tagging efficiencies for the light u, d, s quarks together and c quark, ϵ_dus and ϵ_c, were taken from the simulation, while the one for b quarks, ϵ_b, was measured from the data. The purities, P_f, were calculated from these efficiencies. Similarly the charge separations, $\delta_{\mathrm{d,u,s,c}}$, were taken from the simulation and δ_b was measured. The angular correction factors, η_f, have all been used from the Monte Carlo prediction. The relation between $A_{FB}^{\mathrm{b\bar{b}}}$ and $A_{FB}^{\mathrm{c\bar{c}}}$ was taken from the SM prediction and up type (down type) quark universality was assumed. Consistency of the results over a wide range of κ choices ($\kappa = 0.3, 0.5, 0.8, 1, 1.2, 2.1$) is used to justify the precision of the results.

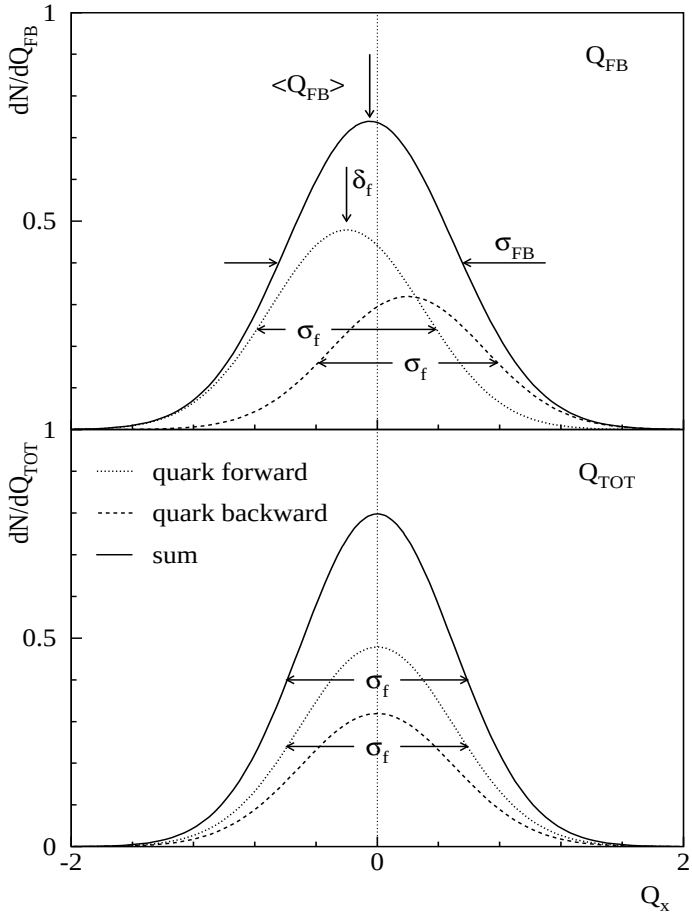

Figure 1: Sketch of the principle of the $\langle Q_{FB} \rangle$ and the $\delta_{\rm f}^2$ measurement for a single (down type) flavour f. $\sigma_{\rm f}$ is the RMS of the Q_{TOT} ($\rightarrow \sigma_{TOT}^{\rm f}$) distribution or of the Q_{FB} distribution for quarks going only to the forward (backward) direction, respectively. σ_{FB} is the RMS of the overall Q_{FB} ($\rightarrow \sigma_{FB}^{\rm f}$) distribution.

2 Detector description and event selection

2.1 The DELPHI detector

The DELPHI detector has been described in detail in [2]. In its coordinate system the z-axis is the direction of the e^- beam. The radius R and the azimuth ϕ are defined in the plane perpendicular to z and the polar angle θ is 0 along z. Only the detector components of relevance for this analysis are mentioned here.

In the barrel part a set of cylindrical detectors, coaxial with the beam direction and inside a 1.2 T solenoidal magnetic field, are devoted to the measurement of the charged particle tracks. The innermost is the Vertex Detector (VD) [3], located just outside the beam pipe. It consists of three concentric layers of silicon micro-strip detectors at average radii of 6.3 cm, 8.8 cm and 10.9 cm from the interaction region. For polar angles of $44^\circ \leq \theta \leq 136^\circ$ a particle crossed all three layers. Until 1993 it provided only measurements of the $R\phi$ coordinate. In 1994 the innermost and the outermost VD layers were equipped with double-sided silicon detectors, which also measured the z coordinate. At the same time the angular acceptance for the innermost layer was enlarged to $25^\circ \leq \theta \leq 155^\circ$.

Outside the VD, between 12 cm and 28 cm of radius, there is the Inner Detector (ID), which includes a jet chamber providing up to 24 $R\phi$ measurements and five layers of proportional chambers providing both $R\phi$ and z information. The ID covers the θ range between 29° and 151°. It is surrounded by the Time Projection Chamber (TPC), the main DELPHI tracking device, which is a cylinder of 3 m length, an inner radius of 30 cm and an outer radius of 122 cm. The ionization charge produced by particles crossing the TPC volume is drifted to the edges of the detector where it is measured in a proportional chamber. Up to 16 space points can be measured, for $39° < \theta < 141°$. Outside this region, and up to 21° and to 159°, a track can be reconstructed using at least 3 points. Additional $R\phi$ measurements on the charged particle tracks are provided by the Outer Detector (OD), which lies between radii of 198 cm and 206 cm and consists of five layers of drift cells. In the forward region two sets of planar wire chambers (FCA, FCB), at ± 160 cm and at ± 270 cm in z, provide measurements of low angle particle trajectories.

The electromagnetic calorimeters, the High Density Projection Chamber (HPC) in the barrel and the Forward Electro-Magnetic Calorimeter (FEMC) in the forward region, are used to measure electrons and photons.

2.2 The sample of hadronic events

The cuts applied to tracks measured in the detector and to events (see Tab.1,2) are optimized to assure well measured tracks for the analysis and to reduce the background arising from lepton and $\gamma\gamma$ events as well as from beam-gas or beam-wall interactions.

charged particle momentum	$\geq$ 0.4 GeV/c
neutral particle energy	$\geq$ 0.5 GeV
length of tracks measured only with TPC	$\geq$ 30 cm
polar angle for charged (neutral) particles	$\geq$ 20°(11°)
relative uncertainty of the momentum measured	$\leq$ 100 %
impact parameter ($R\phi$)	$\leq$ 4 cm
$\sin\theta\times$ impact parameter (z)	$\leq$ 8 cm

Table 1: Cuts to select well measured tracks.

After the selection the contribution from background events is negligible. Further cuts were applied to require a good measurement of the forward and backward hemisphere charges. Events containing one or more particles, either charged or neutral, with momentum greater than 50 GeV were discarded.

total charged energy	$\geq 0.15 \times \sqrt{s}$
hemisphere charged energy	$\geq 0.03 \times \sqrt{s}$
total charged multiplicity	$\geq$ 7
hemisphere charged multiplicity	$\geq$ 1
polar angle of the Thrust axis	$\in [35°, 85°]$

Table 2: Cuts to select hadronic events ; $\sqrt{s}$: cms energy.

The angular acceptance is reduced because of a decreasing b-tagging capability in the forward region due to the limited coverage of the microvertex detector. It is restricted as well by detector effects entering into the measurement of the hemisphere charge. The angle between the momentum vector and magnetic field limits the momentum resolution. The TPC middle plate causes problems for the momentum measurement and charge identification near $\theta = 90°$.

All data collected during the years 1992 up to 1995, on and close to the Z^0 peak, corresponding to $3.5 \cdot 10^6$ hadronic events were used in this analysis. The average centre-of-mass energy on peak is 91.24 GeV .

2.3 Tagging of $b\bar{b}$ events with an impact parameter method

To select a sample enriched in $b\bar{b}$ events an enhanced impact parameter method was used. This technique is based on the well established impact parameter method which was originally proposed by ALEPH [4] and then adopted in DELPHI [5–7].

To reach an improved separation capability, especially b from c events, additional information like the effective mass and energy of the particles reconstructed at a secondary vertex, was included [7].

The DELPHI Vertex Detector [3,8], allows a very precise measurement of spatial points along the charged particles path. For data taken in 1992 and 1993 vertices were fitted on an event by event basis [5,7], using the two dimensional information of the microvertex detector, while the individual impact parameters were evaluated in the plane perpendicular to the colliding beams. For data taken since 1994 the then available z information was used in addition to calculate the vertex and the impact parameters.

For this analysis a combined probability variable, b_{tag}, was used. $b\bar{b}$ events tend to have higher b_{tag} values whereas non-b events are peaked at smaller values (Fig.2) .

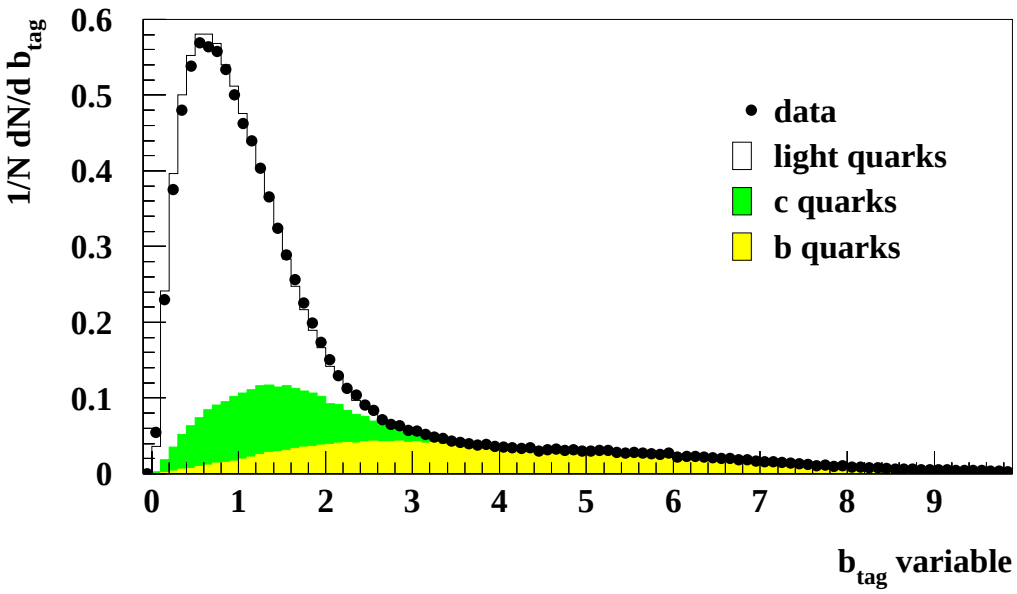

Figure 2: Comparison between data and simulation of the normalised number of events versus the b_{tag} variable (for 1994 data);
light quark, c quark, and b quark events are shown separately for the simulation.

Samples of events were selected by cutting on b_{tag}, where the corresponding b efficiencies (purities) decrease (increase) with higher cut values, respectively. Note that the samples selected are highly correlated because the events selected with a certain cut value are a subsample of the events selected for all lower cut values used.

The b efficiency, ϵ_b, is defined as the probability of selecting a $b\bar{b}$ event inside a data sample, and the b purity, P_b, is the fraction of $b\bar{b}$ events in the selected sample. ϵ_b is measured from the data using

$$\epsilon_b(cut) = \frac{\mathcal{F}(cut) - R_c \times \epsilon_c(cut) - (1 - R_c - R_b) \times \epsilon_{dus}(cut)}{R_b} \tag{9}$$

where $\mathcal{F}$ is the fraction of selected events at a given cut value. ϵ_{dus} and ϵ_c are the selection efficiencies for the light flavours and the charm events, which are both obtained from the simulation. R_c and R_b are the fractions of $c\bar{c}$ and $b\bar{b}$ events produced in hadronic Z^0 decays and are fixed to their Standard Model values of 0.1720 (0.2158) for R_c (R_b). The corresponding purities can be calculated using Eqn.10 .

$$P_f(cut) = \epsilon_f(cut) \times \frac{R_f}{\mathcal{F}(cut)} \tag{10}$$

Accurate tuning of the Monte Carlo sample to the data was performed [5,7] in order to estimate the efficiencies correctly. The data collected in different years were treated separately, due to the changes in the detector.

3 Determination of the charge separations

3.1 Charge separations of light flavours

Reliable values of the light flavour charge separations, their errors and correlations have been determined using the framework of Monte Carlo fragmentation models [9]. The ARIADNE parton shower ansatz combined with the JETSET fragmentation generator currently gives the best overall description of hadronic and identified particle distributions [10–13]. Therefore this model with heavy quark decays adjusted to match recent data [15] , was chosen for the calculation of the quark charge separations. In the following this model will be referred to as the J/A fragmentation model.

A local approximation procedure [9,12] was applied to determine the charge separations of light and charm flavours. The algorithm allows variations of different model parameters important for the considered observable to be studied quickly. A simultaneous variation of these model parameters is possible, because the influence of their correlation was also considered. The relevant calculations were efficiently performed using a quadratic analytic substitution of the Monte Carlo model.

Therefore the model dependence of *all charge separations* and also of *all related bins of all input distributions*, like particle rates and momentum spectra, event shapes etc. were approximated by the following analytic expression, $X_{MC}(p_1, ..., p_n)$, quadratic in the n model parameters p_i :

$$X_{MC}(p_1, ..., p_n) = A_0 + \sum_{i=1}^{n} B_i p_i + \sum_{i=1}^{n} C_i p_i^2 + \sum_{i=1}^{n-1} \sum_{j=i+1}^{n} D_{ij} p_i p_j \tag{11}$$

The coefficients D_{ij} allow for correlations among the model parameters. The $N = \frac{n}{2}(n + 3)+1$ coefficients A_0, B_i, C_i and D_{ij} for each bin were determined from a linear fit of Eqn.11

to 200 sets of Monte Carlo distributions generated with different model parameters. Each of the Monte Carlo sets consists of 500,000 events. The model parameters were chosen at random in a parameter hypercube defined by the parameter intervals given in Tab.3 .

No.	Parameter	Code	default	interval gen.	optimal
1	Lund a	PARJ(41)	0.5	0.3 - 1.0	0.176
2	Lund b	PARJ(42)	0.5	0.1 - 0.8	0.632
3	σ_q	PARJ(21)	0.39	0.36 - 0.42	0.357
4	Λ_{QCD}	PARA(1)	0.24	0.21 - 0.27	0.357
5	p_t^{QCD}	PARA(3)	0.7	0.3 - 0.9	0.531
6	γ_s	PARJ(2)	0.29	0.26 - 0.32	0.280
7	$P(qq)/P(q)$	PARJ(1)	0.1	0.085 - 0.115	0.102
8	$P(us)/P(ud)/\gamma_s$	PARJ(3)	0.5	0.3 - 0.7	1.083
9	$P(ud1)/P(ud0)/3$	PARJ(4)	0.07	0.04 - 0.10	0.046
10	Popcorn	PARJ(5)	0.5	0.06 - 4.5	0.788
11	add. baryon suppr.	PARJ(19)	0.5	0.1 - 0.9	0.397
12	$P(^1S_0)_{ud}$	—	—	0.2 - 0.5	0.398
13	$P(^3S_1)_{ud}$	—	—	0.2 - 0.5	0.382
14	$P(^1S_0)_s$	—	—	0.2 - 0.5	0.483
15	$P(^3S_1)_s$	—	—	0.2 - 0.5	0.248

Table 3: ARIADNE and JETSET parameters related to charge separations. Interval gen. denotes the interval in which the parameters of the initial Monte Carlo sets have been chosen.

The precision of this procedure was tested by comparing the results of the analytic substitution with the real Monte Carlo answer. The average precision for all bins (including those with small statistics) was found to be 1.2% and for the charge separations (average statistical precision 0.3%) it was found to be 0.5%. No systematic bias of the predictions was observed.

In order to determine optimal model parameters $\vec{p}_{opt}$ and the corresponding charge separations the analytic model was fitted by minimizing $\chi^2 = \sum((X_{MC} - X_{data})/\sigma_{data})^2$ [14] using different sets of data distributions given in Tab.4 . Due to imperfections of the data and the model the χ^2/N_{df} for some distributions is unacceptably large. For these distributions the errors were rescaled according to the prescription given in [15] such that $\chi^2/N_{df} = 1$ and the fit was repeated. The optimized parameters are given in Tab.3 . Some of the optimal values for model parameters are not inside the given range. Therefore it was explicitly checked by production of Monte Carlo events with these optimal parameters, that the resulting analytic approximation is still in good agreement with the Monte Carlo prediction.

To obtain the systematic error of the charge separations, δ_{f}, due to uncertainties in the fragmentation model, all parameters were systematically varied in the 15-dimensional hyperspace. The expected Monte Carlo answer is given by Eqn.11 and compared to the data sets given in Tab.4 . The corresponding χ^2 reflects the quality of the chosen

distribution	data set												
	1	2	3	4	5	6	7	8	9	10	11	12	13
x_p [D] ρ^0 [A,D] ω [A] f^0, f^2 [D] K^{*0} [A,D,O] $K^{*\pm}$ [A,D,O] Proton [A,D] Ξ, Ξ^* [A] $y(p) - y(\bar{p})$ [A] $y(\Lambda) - y(\bar{\Lambda})$ [O] Δ^{++} [D,O] Λ^0 [A,D] Σ_{1385} [D,O]	•	•	•	•	•	•	•	•	•	•	•	•	•
charged multiplicity							•	•	•	•	•	•	•
Thrust, Major, Minor [D] $p_t^{in/out}$ (Thrust) [D] Rapidity (Thrust) [D] $D_{2,3}$ Durham [D]	•		•		•		•		•		•		•
Spher., Aplan., Plan. [D] $p_t^{in/out}$ (Spher.) [D] Rapidity (Spher.) [D] $D_{2,3}$ Jade [D]		•		•		•		•		•		•	•
K^0 [A]	•	•			•	•	•	•			•	•	•
$K^{\pm}$ [A]			•	•	•	•			•	•	•	•	•

Table 4: Combinations of input data used for the determination of the charge separations (data set 13) and for the systematic cross check (data set 1-12). The • denotes the data belonging to the dataset. [A] means ALEPH Measurement, [D] means DELPHI Measurement and [O] means OPAL Measurement.

parameter setting. A cut in χ^2 is performed to select all parameter settings within one standard deviation around the optimum. For all parameter settings which survive the cut in χ^2 the charge separations δ_f are also calculated using Eqn.11 . The scattering of the charge separations reflects the uncertainty of the Monte Carlo model.

A further systematic error of this approach was estimated by using 12 alternative combinations of input data for the determination of the central parameters. The different combinations are presented in Tab.4 . They were selected in order to account for the fact that the K^0 and $K^{\pm}$ spectra cannot be perfectly simultaneous described, nor can the charged multiplicity and the x_p-distribution [12]. Event shape distributions alternatively linear or quadratic in the particle momenta were chosen. Data set 13 will be referred to as the reference data set in the following, because it contains a fit to all distributions, and is mainly used for calculating the results.

The influence of the detector was then considered by folding the charge flow distributions with a detector response matrix. This matrix was determined using the full simulation of the DELPHI apparatus. For a generated charge flow in a given bin it determines the probability to measure the charge flow in any other bin of the distribution. As this matrix can only be determined for events which were accepted in the analysis, a further correction factor was applied to account for a possible bias due to the events rejected by the measuring process or cuts applied in the analysis.

The mean values of the charge separations $\delta_{\mathrm{d,u,s,c}}$ using the reference data set are given in Tab.5 for the detector setting of 1994.

κ	δ_{d}	δ_{u}	δ_{s}	δ_{c}
0.3	-0.1406	0.2392	-0.1816	0.1677
0.5	-0.1638	0.2870	-0.2308	0.1735
0.8	-0.1963	0.3540	-0.3005	0.1746
1.0	-0.2151	0.3917	-0.3408	0.1734
1.2	-0.2299	0.4229	-0.3753	0.1717
2.1	-0.2708	0.4075	-0.4692	0.1615

Table 5: Charge separations as determined with the J/A model and folded with the DELPHI detector performance of 1994.

Because the charge separations were folded with the response of the DELPHI detector they cannot be directly compared to the corresponding results of other experiments. Only the ratios of the different flavours should be compatible. Comparing the different years of data taking, the values change slightly, due to a different acceptance of tracks and events from the different flavours.

The influence of the b-tagging leads to a bias in the charge separations. A correction was determined from the DELPHI simulation and accounts for differences in the b efficiency dependence. At the working point of $\epsilon_{\mathrm{b}} = 75\%$ and $P_{\mathrm{b}} = 92\%$, the corrections which were applied are given in Tab.6 for the different quark flavours.

κ	$\mathcal{C}_{\mathrm{d}}$	$\mathcal{C}_{\mathrm{u}}$	$\mathcal{C}_{\mathrm{s}}$	$\mathcal{C}_{\mathrm{c}}$
0.3	0.65 ± 0.05	0.80 ± 0.04	0.72 ± 0.05	0.86 ± 0.01
0.5	0.67 ± 0.05	0.82 ± 0.04	0.74 ± 0.04	0.81 ± 0.02
0.8	0.69 ± 0.05	0.84 ± 0.04	0.76 ± 0.04	0.71 ± 0.02
1.0	0.70 ± 0.06	0.86 ± 0.04	0.76 ± 0.04	0.65 ± 0.02
1.2	0.72 ± 0.06	0.87 ± 0.04	0.76 ± 0.04	0.58 ± 0.03
2.1	0.75 ± 0.07	0.91 ± 0.05	0.76 ± 0.05	0.37 ± 0.05

Table 6: Correction factors due to b-tagging bias with their statistical error on $\delta_{\mathrm{d,u,s,c}}$ for different κ's at the working point for 1994 data ($\mathcal{C}_{\mathrm{f}} = \delta_{\mathrm{f}}(P_{\mathrm{b}})/\delta_{\mathrm{f}}$; $P_{\mathrm{b}} = 92\%$).

To account for the angular dependence of the differential asymmetry, the $A_{FB}^{\mathrm{b\bar{b}}}$ measurement is performed in 4 different bins of $\theta_{\vec{T}}$. The light quark charge separations are extracted using the complete selected region. Correction factors to account for the different $\theta_{\vec{T}}$ bins are taken from the simulation and are listed in Tab.7 . These corrections are small, independent of the b-tagging and show little dependence on κ and on the year of data taking.

$\theta_{\vec{T}}$	$\mathcal{C}_{\rm d}$	$\mathcal{C}_{\rm u}$	$\mathcal{C}_{\rm s}$	$\mathcal{C}_{\rm c}$
$75^\circ - 85^\circ$	1.03 ± 0.17	0.94 ± 0.10	1.06 ± 0.12	0.91 ± 0.06
$65^\circ - 75^\circ$	0.88 ± 0.16	1.00 ± 0.10	1.02 ± 0.12	1.01 ± 0.06
$50^\circ - 65^\circ$	0.91 ± 0.15	0.96 ± 0.09	0.95 ± 0.10	1.04 ± 0.06
$35^\circ - 50^\circ$	1.26 ± 0.20	1.17 ± 0.12	0.98 ± 0.14	1.03 ± 0.08

Table 7: Correction factors due to angular dependence with their statistical error on $\delta_{\rm d,u,s,c}$ for different $\theta_{\vec{T}}$ bins for 1994 data ($\mathcal{C}_{\rm f} = \delta_{\rm f}(\theta_{\vec{T}})/\delta_{\rm f}$; $\kappa = 0.8$).

3.2 b charge separation

The b charge separation was measured from the widths of the charge flow and the total charge distributions with very small input from the simulation. This avoids a dependence on the poorly known B hadron decays.

A single measurement of the hemisphere charge can be regarded as sum of three independent terms:

$$Q_{\rm f} = \frac{\delta_{\rm f}}{2} + \frac{E_{\rm f}}{2} + S_{\rm f} \qquad Q_{\bar{\rm f}} = \frac{-\delta_{\rm f}}{2} + \frac{E_{\bar{\rm f}}}{2} + S_{\bar{\rm f}} \tag{12}$$

where $E_{\rm f}$ $(=E_{\bar{\rm f}})$ is a non vanishing (positive) bias due to hadronic re-interactions in the detector material and $S_{\rm f(\bar{f})}$ accounts for statistical variations of $Q_{\rm f(\bar{f})}$, thus $\langle S_{\rm f(\bar{f})} \rangle = 0$. From the two equations above one obtains:

$$\sum_{\rm f=d,u,s,c,b} P_{\rm f}\delta_{\rm f}^2 = \sigma_{FB}^2 - \sigma_{TOT}^2 + \langle Q_{FB} \rangle^2 + \underbrace{\sum_{\rm f=d,u,s,c,b} P_{\rm f}(4\langle S_{\rm f} S_{\bar{\rm f}} \rangle + E_{\rm f}^2) - (\sum_{\rm f=d,u,s,c,b} P_{\rm f} E_{\rm f})^2}_{\rm MC_{cor}} \tag{13}$$

This equation describes the relation between $\delta_{\rm b}$ and the other measurable quantities. Most of the right hand side of this equation can be extracted from data, apart from the last terms, marked with the under brace. They are numerically small and can be safely estimated from simulation. It should be noted that the $E_{\rm f}$ terms cancel completely in Eqn.13 if $P_{\rm b} = 1$ or if $E_{\rm f}$ is flavour independent. Left over are the $\langle S_{\rm f} S_{\bar{\rm f}} \rangle$ terms accounting for the small hemisphere-hemisphere charge correlation, which is due to charge conservation, the common Thrust axis and occasional particle crossovers between hemispheres.

The right hand side of Eqn.13 was evaluated in samples of increasing b purity, which were obtained by selecting events lying above a certain $\rm b_{tag}$ value. The b charge separation can be extracted directly when subtracting the background part $\sum_{\rm f \neq b} P_{\rm f}\delta_{\rm f}^2$ and separating $\delta_{\rm b}$.

The measured $\delta_{\rm b}$ is shown for the considered b purity range in Fig.3 c) for two different κ values. In this high purity region the resulting $\delta_{\rm b}$ is nearly stable although some bias due to the applied b-tagging is expected.

The measured mean squared charge separation (Fig.3 a)) and the term deduced from the Monte Carlo, which includes the hemisphere correlation term, (Fig.3 b)) are shown in addition. Note that the points are highly correlated. This extraction procedure was checked on simulated data where it reproduced the input charge separation correctly.

The extracted $\delta_{\rm b}$ values used for the analysis at a working point of $P_{\rm b} = 92\%$ are given in Tab.8 for the different years. The error of the charge separation due to the systematics of the determination of the light and charm charge separation is always more than one order of magnitude smaller than the statistical one.

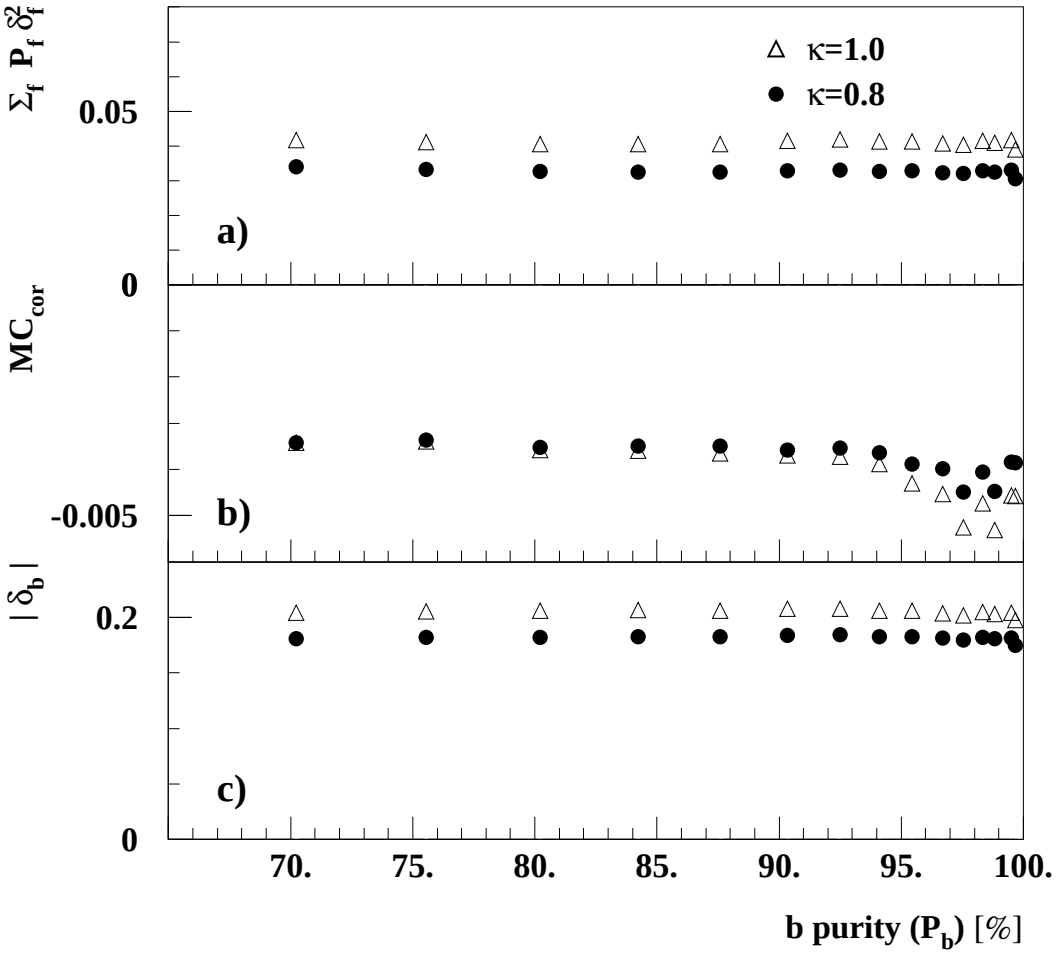

Figure 3: Measurement of $\delta_{\rm b}$ for different κ values. a) : $\sum_{\rm f} P_{\rm f}\delta_{\rm f}^2$, b) : Monte Carlo correction $\mathrm{MC_{cor}}$, c) : calculated $\delta_{\rm b}$

year	$\delta_{\rm b}(\kappa = 0.3)$	$\delta_{\rm b}(\kappa = 0.5)$	$\delta_{\rm b}(\kappa = 0.8)$
92	-0.1184 ± 0.0026	-0.1470 ± 0.0029	-0.1871 ± 0.0039
93	-0.1191 ± 0.0031	-0.1463 ± 0.0035	-0.1850 ± 0.0048
94	-0.1166 ± 0.0017	-0.1446 ± 0.0019	-0.1843 ± 0.0026
95	-0.1176 ± 0.0030	-0.1452 ± 0.0033	-0.1838 ± 0.0046
year	$\delta_{\rm b}(\kappa = 1.0)$	$\delta_{\rm b}(\kappa = 1.2)$	$\delta_{\rm b}(\kappa = 2.1)$
92	-0.2114 ± 0.0048	-0.2331 ± 0.0057	-0.2992 ± 0.0092
93	-0.2079 ± 0.0058	-0.2282 ± 0.0070	-0.2882 ± 0.0114
94	-0.2081 ± 0.0032	-0.2289 ± 0.0039	-0.2882 ± 0.0064
95	-0.2069 ± 0.0056	-0.2273 ± 0.0067	-0.2854 ± 0.0111

Table 8: Calculated $\delta_{\rm b}$ values at the working point for the 4 years of data taking. The error due to the systematics of the determination of the light and charm charge separation varies between 0.0001 and 0.0002 .

Similarly to the light and charm charge separation case correction factors which account for the different $\theta_{\vec{T}}$ bins are taken from the simulation (Tab.9). The variation of the correction factors with increasing $P_{\rm b}$ and the dependence on κ is very small. Within their statistical errors they are equal for the different years of data taking.

$\theta_{\vec{T}}$	$\mathcal{C}(\kappa = 0.3)$	$\mathcal{C}(\kappa = 0.5)$	$\mathcal{C}(\kappa = 0.8)$
$75° - 85°$	0.963 ± 0.010	0.965 ± 0.009	0.967 ± 0.009
$65° - 75°$	1.008 ± 0.009	1.006 ± 0.009	1.005 ± 0.009
$50° - 65°$	1.024 ± 0.008	1.024 ± 0.007	1.024 ± 0.008
$35° - 50°$	0.993 ± 0.010	0.992 ± 0.009	0.991 ± 0.009
$\theta_{\vec{T}}$	$\mathcal{C}(\kappa = 1.0)$	$\mathcal{C}(\kappa = 1.2)$	$\mathcal{C}(\kappa = 2.1)$
$75° - 85°$	0.968 ± 0.009	0.968 ± 0.010	0.969 ± 0.011
$65° - 75°$	1.005 ± 0.009	1.006 ± 0.010	1.006 ± 0.011
$50° - 65°$	1.024 ± 0.008	1.023 ± 0.008	1.022 ± 0.009
$35° - 50°$	0.991 ± 0.009	0.991 ± 0.010	0.991 ± 0.011

Table 9: Correction factors to $\delta_{\rm b}$ due to angular dependence with their statistical errors for different $\theta_{\vec{T}}$ bins for 1994 data.

For completeness $\langle Q_{TOT} \rangle$, H (defined in Eqn.14 below) and $\sigma^2_{FB} - \sigma^2_{TOT}$ are shown in Fig.4, because they enter in the determination of $\delta_{\rm b}$. The quantity $\langle Q_{TOT} \rangle = \sum_{\rm f} P_{\rm f} E_{\rm f}$ was taken from the simulation because of the cancellation effect mentioned.

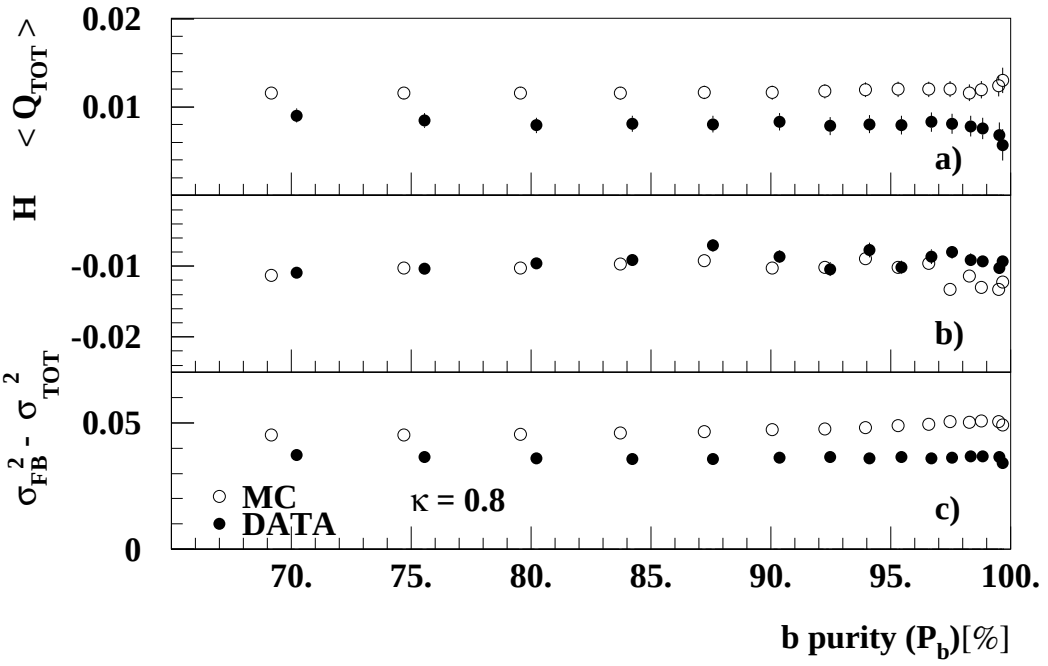

Figure 4: A comparison of data and simulation for $\langle Q_{TOT} \rangle$, H and $\sigma^2_{FB} - \sigma^2_{TOT}$ with $\kappa = 0.8$ for the year 1994.

The discrepancies in the $\langle Q_{TOT} \rangle$ measurement are due to an inaccurate description of the secondary interactions in the simulation and are considered in the systematic studies.

The deviations enter in most of the hemisphere charge related observables. The disagreement in the $\langle Q_{TOT} \rangle$ observable is less important because the value enters only via the numerically small Monte Carlo correction term.

A good control of the hemisphere-hemisphere correlation is also important for the δ_b extraction. This correlation term is strongly related to the observable $\langle Q_F Q_B \rangle$, which includes also the discrepancies in the secondary interaction description. Therefore a modified observable, H, where these differences are mostly reduced by the subtraction of the $\langle Q_{TOT} \rangle$ term, is considered :

$$\mathrm{H} = \langle Q_F Q_B \rangle - \langle Q_{TOT} \rangle^2 / 4 \tag{14}$$

A sufficient agreement between data and simulation was found and ensures the validity of the δ_b determination. The remaining differences are included in the systematic uncertainties.

$\sigma^2_{FB} - \sigma^2_{TOT}$ was taken from the data and the deviation between data and simulation reflects that the δ_b value inside the simulation differs from the measured one. This is expected and due to the difficulty of implementing the poorly known B hadron decays in the Monte Carlo description.

4 The measurement of $A^{b\bar{b}}_{FB}$

$A^{b\bar{b}}_{FB}$ was determined mainly from $\langle Q_{FB} \rangle$ using Eqn.6. To profit from the angular dependence the calculation was performed for 4 $\theta_{\vec{T}}$-bins, $35° - 50°$,$50° - 65°$, $65° - 75°$ and $75° - 85°$, separately and combined later in a χ^2-fit procedure. $\langle Q_{FB} \rangle$ is shown in comparison with the simulation in Fig.5 for the full angular range. The difference between data and simulation, which is similar for all $\theta_{\vec{T}}$-bins, is due to different underlying charge separations as mentioned before and to different input asymmetries.

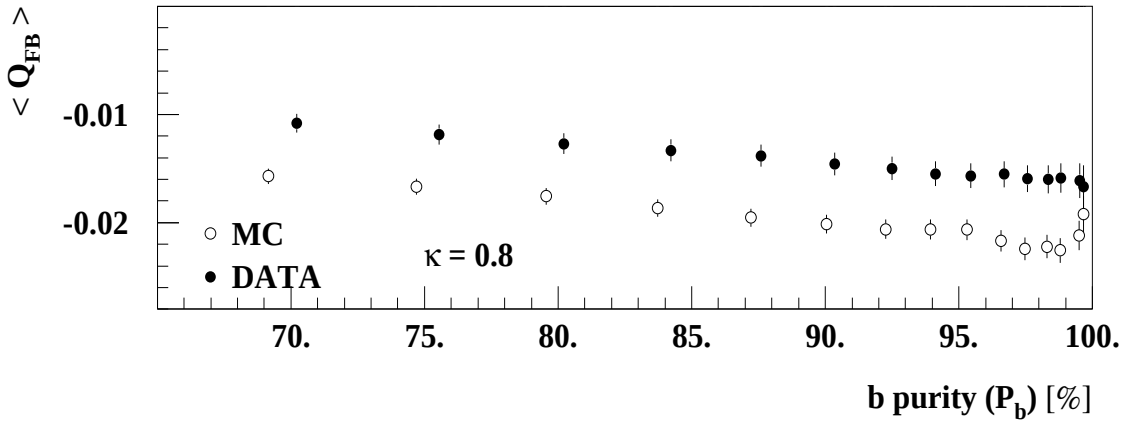

Figure 5: $\langle Q_{FB} \rangle$ as obtained from data and simulation for $\kappa = 0.8$ for 1994 data.

The determination of the other quantities entering in Eqn.6 and Eqn.9 is discussed below with the exception of the charge separations which were discussed already.

4.1 The tagging efficiencies ϵ_f and purities P_f

The effects of different acceptance for the quark flavours depending on the b-tagging applied were estimated from the simulation. The change of the b efficiency due to sys-

tematic uncertainties in the contents of the light and charm flavours requires detailed systematic studies (see section 5).

The efficiencies for light and charm quarks are taken from the simulated data sample and enter in the measurement of the b efficiency, $\epsilon_{\rm b}$, which is mainly extracted from the data using Eqn.9. $R_{\rm b}$ and $R_{\rm c}$ are taken from the Standard Model prediction. The corresponding purities, $P_{\rm f}$, are then calculated using Eqn.10.

The contribution of charm events has to be checked in detail because charm events have an opposite asymmetry compared to the down type b quark. Long lived charm fragmentation products may be found even after applying a high cut on the b-tagging probability. At large b purity ($P_{\rm b} = 92\%$) about 75% of the remaining background is due to charm events. For example, the lifetimes and fractions of D mesons, in c events were checked carefully.

4.2 The angular correction factor $\eta_{\rm f}$

The angular acceptance of the analysis is limited below 35° in polar angle, due to decreasing b-tagging capability, detector acceptance and decreasing momentum resolution of the tracking system at small angles. The part around 90° was rejected because the measurement of $\delta_{\rm b}$ is distorted due to detector material effects and in addition does not contribute to the asymmetry measurement. As the differential asymmetry depends upon the polar angle, a correction factor η was applied. Neglecting mass and gluon radiation effects this correction factor can be written as:

$$\eta_1^{\rm f} \;=\; \frac{8}{3}\frac{\int_0^1 \epsilon_{\rm f}(\cos\theta)\cos\theta \; d\cos\theta}{\int_0^1 \epsilon_{\rm f}(\cos\theta)(1+\cos^2\theta) \; d\cos\theta} \tag{15}$$

$\epsilon_{\rm f}(\cos\theta)$ is the flavour dependent selection efficiency. As the Thrust axis ($\vec{T}$) is considered as the reference direction, no QCD effects are included. For b quarks this variable can be measured on data and compared to the simulation.

The radiation of hard gluons for events at initially very small polar angles θ and losses of particles in the dead areas of the detector close to the beam may cause these events to be accepted in the analysis. A correction for this effect, which depends on the amount of gluon radiation, limited angular acceptance and smearing can be calculated as:

$$\eta_2^{\rm f} \;=\; \frac{Q_{FB}^{\rm f}}{\delta_{\rm f} A_{FB}^{{\rm f},gen}} \tag{16}$$

In order to reduce the statistical error of this correction $\eta_2^{\rm f}$ was calculated with an artificially enlarged generated asymmetry of 0.75 assuming a perfectly forward/backward symmetric detector. A breakdown of the different correction factors η for 1994 data is given in Tab.10 in order to depict the magnitude of the different corrections .

flavour	η_1	$\eta_2(\kappa = 0.8)$	flavour	η_1	$\eta_2(\kappa = 0.8)$
d	0.904 ± 0.028	0.950 ± 0.080	u	0.904 ± 0.032	0.956 ± 0.055
s	0.905 ± 0.027	0.912 ± 0.060	c	0.886 ± 0.008	0.943 ± 0.033
b	0.930 ± 0.001	0.930 ± 0.005			

Table 10: Comparison between η_1 and η_2 for the year 1994.

For the determination of the central results η_2 is always used. The QCD correction term can be estimated by the ratio η_2/η_1 and is compatible with 1. This is to be expected as the charge separations should include effects due to gluon radiation.

The rather big errors for the light and c quarks are due to low statistics in the high b purity region and have little influence on the result. The factor η_1 is by construction κ independent, while η_2 shows no κ dependence within errors. Both quantities vary with increasing P_{b} and the values show a slight change for the different years.

4.3 The determination of $A_{FB}^{\mathrm{b\bar{b}}}$

The determination of $A_{FB}^{\mathrm{b\bar{b}}}$ with the data on the Z^0 peak

The angular correction factor η was calculated separately for the $\theta_{\vec{T}}$ bins using Eqn.16 . The purities were also computed for each angular bin. The δ_{b} measurement was performed using the full angular range and then corrected for angular dependence using the simulation. The light and charm quark charge separations were evaluated using an analytic approximation of the Monte Carlo fragmentation model. The resulting values were corrected using the simulation for detector effects, for the b purity dependence and, analogous to δ_{b}, for the angular binning. No additional b mixing correction was applied, because this is already included in the δ_{b} measurement. It was checked that the $A_{FB}^{\mathrm{b\bar{b}}}$ extracted for the different $\theta_{\vec{T}}$ bins are compatible. The relation between $A_{FB}^{\mathrm{b\bar{b}}}$ and $A_{FB}^{\mathrm{c\bar{c}}}$ was taken from the SM and an up/down type quark universality was assumed ($A_{FB}^{\mathrm{b\bar{b}}} = A_{FB}^{\mathrm{s\bar{s}}} = A_{FB}^{\mathrm{d\bar{d}}}$, $A_{FB}^{\mathrm{c\bar{c}}} = A_{FB}^{\mathrm{u\bar{u}}}$).

The determination was performed for 6 κ values and for the full range of P_{b}. The results are highly correlated in both cases. The working point was chosen at $\kappa = 0.8$ and the values of P_{b} in Fig.7 in order to minimize the total error on the $A_{FB}^{\mathrm{b\bar{b}}}$ measurement.

For $\kappa = 0.8$ the variation with P_{b} is given individually for all the years in Fig.6 . Note again that the data points are highly correlated. The working point is marked by the arrow and the central peak value is given by the horizontal line. The extracted $A_{FB}^{\mathrm{b\bar{b}}}$ values are stable and compatible between the years of data taking.

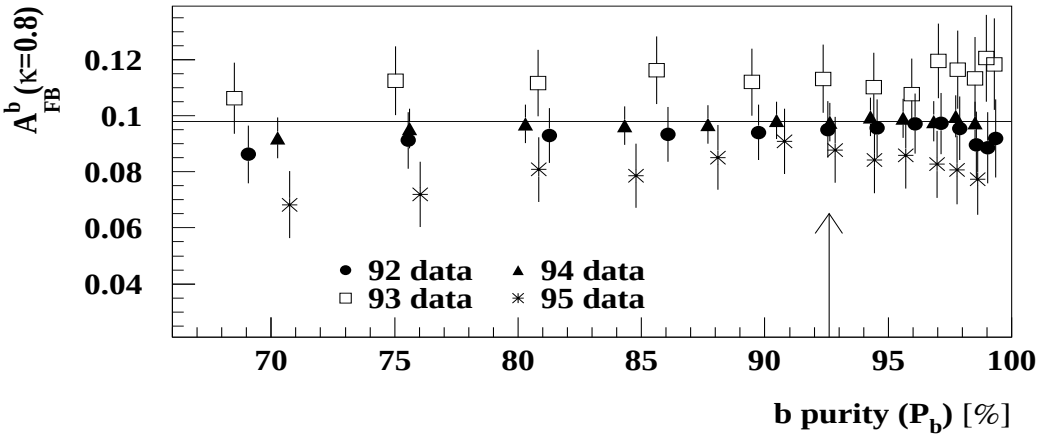

Figure 6: Results of the $A_{FB}^{\mathrm{b\bar{b}}}$ measurement on the Z^0 peak as function of P_{b} with statistical error for $\kappa = 0.8$ for all the years. The horizontal line corresponds to the combined result for the peak value.

For different κ's the results are given at the working point b purity in Fig.7 . Only the statistical errors are shown. The κ dependence slightly differs between the years of data taking, which is due to a different detector response.

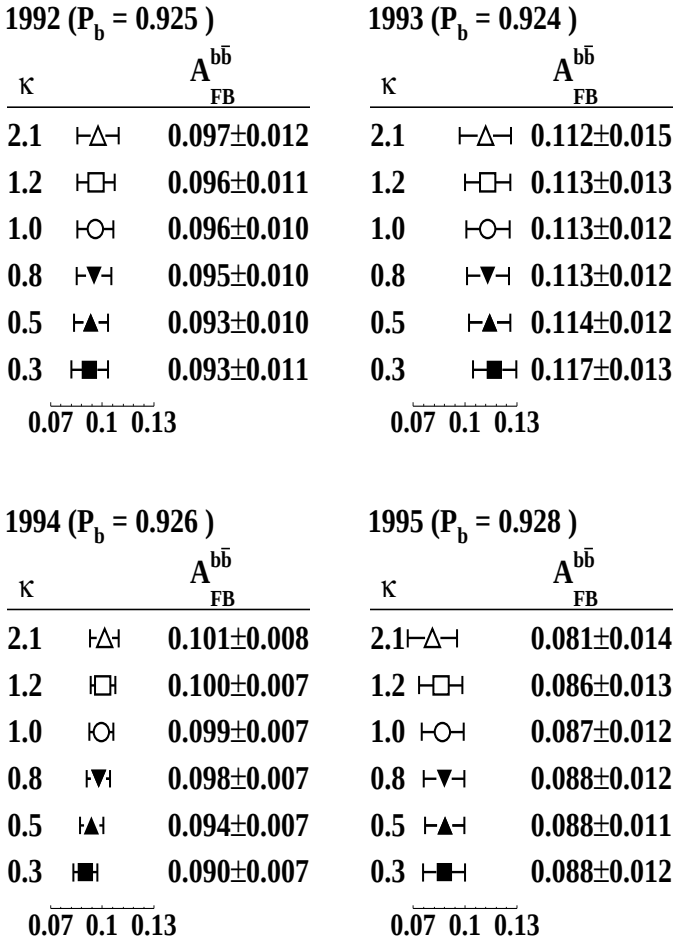

Figure 7: Results of the $A_{FB}^{\mathrm{b\bar{b}}}$ measurement on the Z^0 for different κ values with statistical error. For all years only the selected working point in P_{b} is shown.

The determination of $A_{FB}^{\mathrm{b\bar{b}}}$ with the data close to the Z^0 peak

For the years 93 and 95 the analysis of the data close to the Z^0 peak was performed analogous to the peak data measurements of the same year. Using simulation it was checked that most of the quantities entering in Eqn.6 are energy independent within statistical uncertainties. Therefore only $\langle Q_{FB} \rangle$ was calculated for the data above and below the Z^0 peak separately. All other quantities were evaluated with the peak data or its corresponding simulation. It was checked that the b charge separation, extracted with the data at the Z^0 peak, can be used safely for the data close to the Z^0 .

The final results of the $A_{FB}^{b\bar{b}}$ measurement

The $A_{FB}^{b\bar{b}}$ measurements are summarized in Tab.11 . The results are given with their statistical error at the different average centre-of-mass energies at which LEP has run.

year	# of events	$\sqrt{s}$ [GeV]	$A_{FB}^{b\bar{b}}$
92	505380	91.28	0.095 ± 0.010
93	65620	89.43	0.083 ± 0.026
	346739	91.22	0.113 ± 0.012
	96528	93.01	0.104 ± 0.023
94	986579	91.20	0.098 ± 0.007
95	60052	89.44	0.049 ± 0.026
	321947	91.29	0.088 ± 0.012
	98815	92.90	0.139 ± 0.021

Table 11: Summary of all $A_{FB}^{b\bar{b}}$ measurements with their statistical error.

Combination of these measurements accounting for common errors leads to the final $A_{FB}^{b\bar{b}}$ results for the data recorded on and close to the Z^0 peak. Details on the systematic studies are described in section 5 .

$$A_{FB}^{b\bar{b}}\ (89.55\ \text{GeV}) = 0.068 \pm 0.018(\text{stat.}) \pm 0.0013(\text{syst.})$$
$$A_{FB}^{b\bar{b}}\ (91.26\ \text{GeV}) = 0.0982 \pm 0.0047(\text{stat.}) \pm 0.0016(\text{syst.})$$
$$A_{FB}^{b\bar{b}}\ (92.94\ \text{GeV}) = 0.123 \pm 0.016(\text{stat.}) \pm 0.0027(\text{syst.})$$

The energy dependence of these final $A_{FB}^{b\bar{b}}$ results is shown in Fig.8 . The curve shows the energy dependence of the Standard Model prediction, which is in good agreement with the data points, given with their statistical errors only.

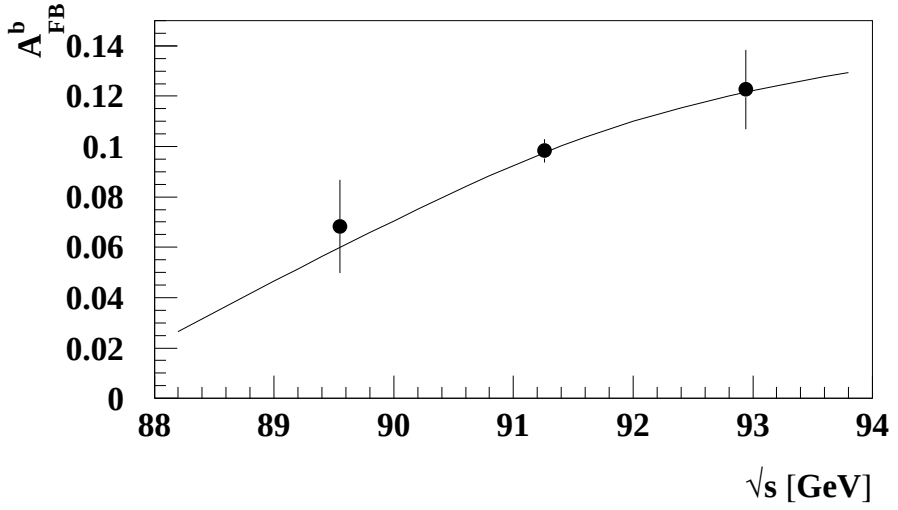

Figure 8: The energy dependence of the final $A_{FB}^{b\bar{b}}$ results with statistical errors in comparison with the Standard Model prediction.

5 Systematic uncertainty estimation

Systematic uncertainties introduced by the b-tagging

In order to determine the systematic uncertainties of the P_f the quantities entering in Eqn.9 were individually studied and varied.

R_c (R_b) was set to the Standard Model values 0.1720 (0.2158) and changed by $\pm 5\%$ ($\pm 0.5\%$) for systematic studies. The dependence of the measured asymmetry values on R_c or R_b is approximately linear. The chosen variation results in systematic uncertainties, which are given in Tab.13 .

The efficiencies for light and charm quarks enter also and a careful study was done as proposed in [16]. Both ϵ_{dus} and ϵ_c depend on the detector performance and were treated for each year separately, as well as the tuning of the b-tagging. Different influences on ϵ_{dus} were studied:

- The gluon splitting into $c\bar{c}$ or $b\bar{b}$ pairs inside light quark events. A change of $\pm 25\%$ for each channel was taken into account [16]. These splittings lead to lifetime information and enter into the b efficiency measurement.
- The K^0 and Λ content in light quark events was varied by $\pm 10\%$ as these contributions may bias the b-tagging.
- To estimate the effect of the detector resolution the probability depending only on the impact parameter information for positive and negative measured impact parameters was used. The difference between the number of events fulfilling the same cut on the event probability distribution for negative measured impact parameters in data and Monte Carlo gives an estimate of the resolution contributing to ϵ_{dus} in the associated bin of the b_{tag} distribution and it corresponding b efficiency.

The tagging efficiency ϵ_c inside the b enriched sample is more substantial than the contributions mentioned before.

- The fractions of D meson production in c events were systematically studied according to the procedure proposed in [16]. The uncertainties were estimated by varying the corrected values inside the uncertainties given in Tab.12 . Each systematic shift of the D^+, D_s, Λ_c contribution was compensated by the D^0 fraction, therefore no extra error is given in that case.
- Shifts induced in ϵ_b, arising from the uncertainties of the D lifetimes were estimated by varying the corrected lifetimes within the errors quoted in Tab.12 .
- The influence of the uncertainty of the average scaled momentum $\langle X_E \rangle$ of the D's was studied by re-weighting the events such that the resulting $\langle X_E \rangle$ changes by $\pm 2\%$ corresponding to the uncertainty of the measurement 0.484 ± 0.008 [16]. This measurement was corrected to a level of no charm produced in gluon splitting events. Nevertheless for systematic studies the 2 or 6 fastest D mesons were taken into account and the resulting variation on the asymmetry turns out to be equal within errors. Events with 2 D mesons are those without c quarks produced in gluon splitting while those with 6 included most of the gluon splitting events.
- The events were re-weighted according to the branching ratio $D \rightarrow K^0X$, depending on the primary D meson inside the c events [15].
- The charged multiplicity in charm events was varied according to the inclusive topological branching ratios measured for D^0, D^+ and D_s [17].

D-Meson	fraction	lifetime [ps]
D^0	0.600	0.415 ± 0.004
D^+	0.233 ± 0.027	1.057 ± 0.015
D_s	0.102 ± 0.029	0.447 ± 0.017
Λ_c	0.063 ± 0.028	0.206 ± 0.012

Table 12: Measurement of D meson fraction inside c quarks and of their lifetimes.

Systematic uncertainties introduced by the η-factor and the QCD correction

For the determination of the central $A_{FB}^{b\bar{b}}$ the definition η_2^f was always used. As mentioned in section 4.2, two different definitions of η^f are reasonable. For an estimate of the systematic uncertainty coming from the selection and the cut in the acceptance region, η_1^f was also considered. The advantage of this definition is that η_1^b can be calculated from the data and from the simulation. A maximum difference of 0.5 % at $P_b = 92\%$ was found considering all years. For the light and c quarks a conservative systematic error of 5% was taken into account, which is the maximum difference between $\eta_1^{f\neq b}$ and $\eta_2^{f\neq b}$, where both numbers were calculated from simulation. The statistical error of all η_2^f calculations is included in the statistical error of the $A_{FB}^{b\bar{b}}$ measurement.

Systematics coming from the Thrust axis resolution were studied and found to be negligible. The experimental thrust axis resolution, when applying the angular acceptance cut, caused an excess of small angle events to enter the acceptance region. The related bias on $A_{FB}^{b\bar{b}}$ was estimated with simulation.

Systematic uncertainties introduced by the dusc charge separations

As mentioned in section 3.1 the uncertainty due to the charge separations was divided into three different sources. The precision of the interpolation procedure, the uncertainty due to the Monte Carlo parameters and the uncertainty due to the choice of the input distributions. The first source gives negligible effects on the result. The second was treated by repeating the $A_{FB}^{b\bar{b}}$ extraction with Eqn.6 with 50 different parameter settings fulfilling the χ^2 cut. Using the reference data set the resulting systematic error on the asymmetry is small. The third was studied by solving this equation with 13 different charge separation data sets tuned separately by using different input distributions. It turns out that the influence of the different data sets is of the same order.

The generated charge separations were folded with an acceptance matrix to account for the influence of the detector response. In a second step a linear correction was applied to account for a possible bias due to the selection. Variation in both steps of the acceptance correction lead to a negligible effect on the asymmetry results.

Several correction factors were applied to the light and charm charge separations. Their statistical errors are contained in the statistical error of the final $A_{FB}^{b\bar{b}}$ measurements. The same treatment was performed to the analogous correction factors applied to the b charge separation.

Systematic uncertainties due to detector effects

The hemisphere-hemisphere correlation term $\langle S_f S_{\bar{f}} \rangle$ is mainly given by H for which a discrepancy of about 20% between data and Monte Carlo was found (depending on the

year). As systematic uncertainty for this correlation term the same order of magnitude was assumed.

To account for inaccurate description of hadronic interactions, the tracks have been reweighted in such a way, that $\langle Q_{TOT} \rangle$ in the simulation becomes equal to the corresponding data value. The full analysis has been performed and the difference in the $A_{FB}^{b\bar{b}}$ measurement has been taken as systematic uncertainty.

Systematic uncertainties due to other effects

The relation between $A_{FB}^{b\bar{b}}$ and $A_{FB}^{c\bar{c}}$ was taken from the SM prediction. For the analysis performed on the Z^0 peak this relation factor was varied by 2%. The corresponding systematic uncertainty is very small. For the measurement close to the Z^0 peak a bigger variation of 10% was assumed.

All the relevant systematic error contributions are summarized in Tab.13 .

Contribution	$\Delta A_{FB}^{b\bar{b}} \times 10^2$ peak	$\Delta A_{FB}^{b\bar{b}} \times 10^2$ peak $-$ 2	$\Delta A_{FB}^{b\bar{b}} \times 10^2$ peak $+$ 2
Charge separation δ_u	± 0.014	± 0.011	± 0.017
Angular correction	± 0.037	± 0.024	± 0.045
$R_b \mp 0.5\%$	± 0.001	± 0.001	± 0.001
$R_c \pm 5\%$	± 0.042	± 0.016	± 0.060
H charge correlation	± 0.110	± 0.076	± 0.160
hadronic interaction	± 0.014	± 0.089	± 0.050
$A_{FB}^{c\bar{c}}/A_{FB}^{b\bar{b}}$(SM)	± 0.002	± 0.015	± 0.060
Detector resolution (light,charm)	± 0.071	± 0.029	± 0.170
Gluon splitting $g \to c\bar{c}$	± 0.005	± 0.002	± 0.008
Gluon splitting $g \to b\bar{b}$	± 0.006	± 0.002	± 0.010
K^0,Λ variation	∓ 0.020	∓ 0.006	∓ 0.027
D^+ fraction in $c\bar{c}$	± 0.032	± 0.013	± 0.049
D_s fraction in $c\bar{c}$	± 0.003	± 0.003	± 0.005
Λ_c fraction in $c\bar{c}$	∓ 0.022	∓ 0.008	∓ 0.038
D^0,D^+,D_s,Λ_c lifetimes	± 0.010	± 0.004	± 0.015
$\langle X_E \rangle$ (fragmentation)	∓ 0.028	∓ 0.007	∓ 0.042
D decay multiplicity	∓ 0.015	∓ 0.004	∓ 0.019
$BR(D \longrightarrow K^0 X)$	± 0.020	± 0.006	± 0.030
total systematic error	$\pm$ 0.16	$\pm$ 0.13	$\pm$ 0.27

Table 13: Systematic uncertainties and their influence on the $A_{FB}^{b\bar{b}}$ determination.

6 Conclusions

A measurement of $A_{FB}^{\mathrm{b\bar{b}}}$ using an impact parameter tag and a jet charge technique was performed. The analysis includes a data sample of $3.5 \cdot 10^6$ hadronic events collected with the DELPHI detector from 1992 to 1995. The data were analysed as a function of the polar angle in a high b purity region of 92%. The asymmetries for the individual years of data taking were measured.

Combining these independent measurements at the different centre-of-mass energies at which LEP has run yields:

$$A_{FB}^{\mathrm{b\bar{b}}}\ (89.55\ \mathrm{GeV}) \ = \ 0.068 \ \pm 0.018\ (\mathrm{stat.}) \pm 0.0013(\mathrm{syst.})$$

$$A_{FB}^{\mathrm{b\bar{b}}}\ (91.26\ \mathrm{GeV}) \ = \ 0.0982 \pm 0.0047(\mathrm{stat.}) \pm 0.0016(\mathrm{syst.})$$

$$A_{FB}^{\mathrm{b\bar{b}}}\ (92.94\ \mathrm{GeV}) \ = \ 0.123 \ \pm 0.016\ (\mathrm{stat.}) \pm 0.0027(\mathrm{syst.})$$

These measurements are combined taking common errors into account. Applying corrections for QED and photon exchange determines the result of the pole asymmetry to be [16]:

$$A_{FB}^{0,\mathrm{b\bar{b}}} \ = \ 0.1012 \ \pm 0.0047\,.$$

This asymmetry corresponds to an effective weak mixing angle given by:

$$\sin^2\theta^{\mathrm{l}}_{\mathrm{eff}} \ = \ 0.23186 \pm 0.00083\,.$$

Both results are in good agreement with the SM and compatible with the recently published data of other experiments [18–20] and the previous DELPHI result [21].

Acknowledgements

We are greatly indebted to our technical collaborators, to the members of the CERN-SL Division for the excellent performance of the LEP collider, and to the funding agencies for their support in building and operating the DELPHI detector.
We acknowledge in particular the support of
Austrian Federal Ministry of Science and Traffics, GZ 616.364/2-III/2a/98,
FNRS–FWO, Belgium,
FINEP, CNPq, CAPES, FUJB and FAPERJ, Brazil,
Czech Ministry of Industry and Trade, GA CR 202/96/0450 and GA AVCR A1010521,
Danish Natural Research Council,
Commission of the European Communities (DG XII),
Direction des Sciences de la Matière, CEA, France,
Bundesministerium für Bildung, Wissenschaft, Forschung und Technologie, Germany,
General Secretariat for Research and Technology, Greece,
National Science Foundation (NWO) and Foundation for Research on Matter (FOM), The Netherlands,
Norwegian Research Council,
State Committee for Scientific Research, Poland, 2P03B06015, 2P03B03311 and SPUB/P03/178/98,
JNICT–Junta Nacional de Investigação Científica e Tecnológica, Portugal,
Vedecka grantova agentura MS SR, Slovakia, Nr. 95/5195/134,
Ministry of Science and Technology of the Republic of Slovenia,
CICYT, Spain, AEN96–1661 and AEN96-1681,
The Swedish Natural Science Research Council,
Particle Physics and Astronomy Research Council, UK,
Department of Energy, USA, DE–FG02–94ER40817.

References

[1] The LEP Collaborations, Phys. Lett. **B276** (1992) 267.

[2] DELPHI Collaboration, P. Abreu et al., Nucl. Instr. Meth. **A303** (1991) 233;
DELPHI Collaboration, P. Abreu et al., Nucl. Instr. Meth. **A378** (1996) 57.

[3] N. Bingefors et al., Nucl. Instr. Meth. **A328** (1993) 447.

[4] ALEPH Collaboration, D. Buskulic et al., Phys. Lett. **B313** (1993) 535.

[5] G. Borisov and C. Mariotti, Nucl. Instr. Meth. **A372** (1996) 181.

[6] DELPHI Collaboration, P. Abreu et al., Z. Phys. **C65** (1995) 555.

[7] DELPHI Collaboration, P. Abreu et al., CERN-EP/98-180, submitted to E. Phys. J. **C**.

[8] V. Chabaud et al., Nucl. Inst. Meth. **A368** (1996) 314.

[9] U. Flagmeyer, Diplomarbeit, WUD 96-25, Bergische Univ.-GH, Wuppertal (1996).

[10] T. Sjöstrand, Comp. Phys. Comm. **39** (1986) 347;
T. Sjöstrand and M. Bengtsson, Comp. Phys. Comm. **46** (1987) 367.

[11] L. Lönnblad, Comp. Phys. Comm. **71** (1992) 15.

[12] DELPHI Collaboration, P. Abreu et al., Z. Phys. **C73** (1996) 11.

[13] W. Neumann, Dissertation, WUB-DIS 97-11, Bergische Univ.-GH, Wuppertal (1997).

[14] F. James and M. Goossens, Minuit, Function Minimization and Error Analysis, Reference Manual, CERN Program Library Long Writeup, **D506** (1992).

[15] The Particle Data Group, R.M. Barnett et al., Phys. Rev. **D54**, 1, (1996).

[16] The LEP Collaborations, Nucl. Inst. Meth., **A378** (1996) 101;
The LEP Heavy Flavour Working Groupe, Presentation of LEP Electroweak Heavy Flavour Results for Summer 1996 Conferences LEPHF 96-01;
The LEP Heavy Flavour Working Groupe, Input Parameters for LEP electroweak Heavy Flavour Results for Summer 1998 Conferences LEPHF 98-01.

[17] MARK III Collaboration, D. Coffman et al., Phys. Lett. **B263** (1991) 135.

[18] ALEPH Collaboration, R. Barate et al., Phys. Lett. **B426** (1998) 217;
ALEPH Collaboration, R. Buskulic et al., Phys. Lett. **B384** (1996) 414.

[19] L3 Collaboration, M. Acciarri et al., CERN EP/98-134 12 August, 1998 to be published in Phys. Lett. B;
L3 Collaboration, M. Acciarri et al., CERN EP/98-156 10 October, 1998 to be published in Phys. Lett. B.

[20] OPAL Collaboration, K. Ackerstaff et al., Z. Phys. **C75** (1997) 385;
OPAL Collaboration, K. Alexander et al., Z. Phys. **C70** (1996) 357.

[21] DELPHI Collaboration, P. Abreu et al., Z. Phys. **C65** (1995) 569.